ELSEVIER

Journal of Nuclear Materials 248 (1997) 292–298

journal of nuclear materials

Formation and dissolution of oxide film on zirconium alloys in 288°C pure water under γ-ray irradiation

Yoshitaka Nishino [a,*], Masao Endo [a], Eishi Ibe [a], Takayoshi Yasuda [b]

[a] *Power and Industrial Systems R&D Division, Hitachi Ltd., 7-2-1 Omika-cho, Hitachi-shi, Ibaraki-ken 319-12, Japan*
[b] *Hitachi works, Hitachi Ltd., 3-1-1 Saiwai-cho, Hitachi-shi, Ibaraki-ken 317, Japan*

Abstract

Laboratory corrosion tests for zirconium alloys which were based on Zircaloy-2 were performed in 288°C oxygenated pure water for 100 days both with and without ^{60}Co γ-ray irradiation. No nodular oxide was observed. Corrosion weight gains of the alloy which had the lowest nodular corrosion resistance were lower for the irradiated condition than the non-irradiated condition. On the other hand, the alloys which had higher nodular corrosion resistances showed almost the same weight gains for both conditions. Differences of weight gain with and without irradiation were attributed to dissolution of the oxide film in the high temperature water. Dissolution tests of single crystal yttria-doped ZrO_2 indicated that 30–40% larger amounts dissolved into water under the γ-ray irradiation. Low angle incident X-ray diffraction analysis showed that the tetragonal-ZrO_2 fraction in the oxide film was lower with irradiation than without it, especially for the near surface area. The water radiolysis species accelerated the dissolution of the oxide film, especially film on the alloy with lower nodular corrosion resistance. This dissolution led to the lower tetragonal-ZrO_2 fraction and was considered to be one of the factors causing a localized breakdown of the barrier oxide film to make the nodular oxide. © 1997 Elsevier Science B.V.

1. Introduction

Zirconium alloys (Zircaloy) are utilized in light water nuclear reactors as fuel cladding materials, channel boxes, etc. When their corrosion is evaluated, irradiation effects on not only materials, but also on water, should be considered. Water molecules decompose in the radiation field to produce radiolytic species such as H_2O_2, O_2^-, HO_2, HO_2^-, OH, etc. Nodular (localized lens-shape) oxides are observed in irradiated oxygenated water coolants such as found in a boiling water reactor (BWR) in which the water radiolysis species are at much higher concentrations than in low-oxygen coolants of a pressurized water reactor (PWR) [1]. This nodular corrosion has not been observed experimentally in high temperature (280–360°C) water conditions without irradiation. It has been seen in higher temperature (> 500°C) steam corrosion tests. Early studies [2,3] pointed out the possibility that the radiolysis species caused the radiation-enhanced corrosion of the zirconium alloys and a computer simulation code was applied to predict the concentrations of those species. The water radiolysis reactions are very complicated systems. Recent studies [4–7] have revealed aspects of the high temperature water radiolysis, making it possible to predict concentrations of the radiolysis species more precisely. However, the phenomena occurring between water radiolysis species and Zircaloy oxide films still remain unclear. In this study, we have used a laboratory γ-ray irradiation facility to investigate the fundamental aspects of interactions between water radiolysis species and oxide films on Zircaloy.

The γ-ray irradiation affects water and induces its radiolysis, but γ-ray irradiation has few effects on the materials themselves. We measured corrosion weight gains of test coupons and observed oxide films under conditions with and without γ-ray irradiation, in which we were especially interested in dissolution of oxide films into water. Cox and Wu [8,9] reported that a Zircaloy oxide film dissolved in LiOH solutions and this dissolution caused a breakdown of the protective oxide film. We also examined the γ-ray irradiation effect on the dissolution of

* Corresponding author. Tel.: +81-294 235 982; fax: +81-294 231 963; e-mail: yoshi_n@erl.hitachi.co.jp.

PII S0022-3115(97)00126-8

Table 1
Zirconium alloy specimens

No.	Elements (wt%)							Annealing parameter [a]	Nodular corrosion test [b]	
	Sn	Fe	Cr	Ni	O	C	Zr		weight gain (mg/dm^2)	coverage (%)
A	1.50	0.14	0.10	0.06	0.12	0.015	ba.	1.2×10^{-18}	> 3400	100
B	1.43	0.15	0.10	0.05	0.12	0.010	ba.	1.5×10^{-19}	97	0
C	1.47	0.22	0.10	0.09	0.13	0.010	ba.	8.3×10^{-20}	51	0

[a] $\Sigma A_i = \Sigma t \exp(-40\,000/T)$, t = annealing time (h), T = annealing temp. (K).
[b] 520°C, 105 kg/cm^2, 24 h, steam.

zirconium oxide (yttria-doped single crystal) in 288°C pure water and NaOH solution.

2. Experimental

2.1. Specimens

The zirconium alloys studied, which were based on Zircaloy-2, are listed in Table 1. Each specimen was $10 \times 20 \times 0.6$ mm. The nodular corrosion resistance of each alloy was examined in a test at 520°C, with 105 kg/cm^2 steam for 24 h. Specimen A showed the lowest nodular corrosion resistance. No nodular oxide was observed on either specimens B or C. Specimen C showed a lower corrosion weight gain than specimen B.

The specimens were chemically polished in a HNO_3 and HF mixture and immersed in deionized water. Prefilmed specimens (400°C steam, 12 h) were also prepared for corrosion tests in 288°C pure (deionized) water. A prefilming treatment was done for all specimens at the same time.

Single crystals (1 mm thick) of 8 mol% Y_2O_3 stabilized ZrO_2 (YSZ) were provided for the dissolution tests.

2.2. Equipment and procedure

A schematic diagram of the experimental apparatus is shown in Fig. 1. The non-irradiation vessel was surrounded by radiation shields and its radiation field was less than 8 Gy/h. The irradiation vessel was located at the center between the ^{60}Co γ-ray sources and its radiation field was 3.0×10^4 Gy/h. The water temperature in both vessels was controlled at 288 ± 1°C. Dissolved gases in water were removed by high purity argon gas bubbling. Then, dissolved oxygen concentration was controlled to 10 ± 0.1 mg/dm^3 in order to produce higher concentrations of radiolysis species. The corrosion test was carried out for up to 2400 h. Oxide film surfaces and cross sections were observed by scanning electron microscope (SEM) (Hitachi, S-4200 and S-2460N). An atomic force microscope (AFM) (Seiko, SPA-260) was used for surface observations and surface roughness measurements. Crystal structures of oxide films were examined by a low angle incident X-ray diffraction analyzer (XRD) (Rigaku, RU300) with Cu-Kα X-ray.

Dissolution experiments of YSZ were performed in the same apparatus (Fig. 1) for 200 h both in pure water (pH 6.9 at 25°C) and in 4.4×10^{-5} mol/l NaOH (pH 9.6 at

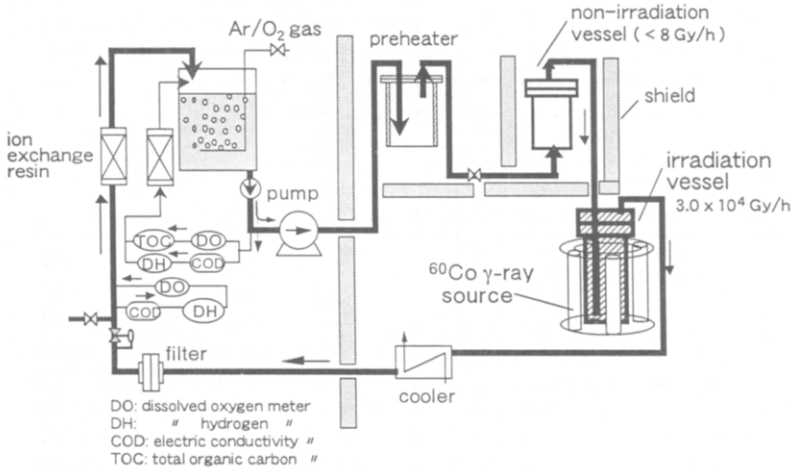

Fig. 1. Experimental apparatus.

Table 2
Radiolysis species and their G-values

Species	G-value (/100 eV)		Oxidant/reductant
	γ-ray[7]	neutron[5]	
H_2	0.60	1.52	red.
O_2	0.0	0.0	ox.
H_2O_2	0.31	1.22	red./ox.
O_2^-	0.0	0.0	ox.
HO_2^-	0.00	0.00	red./ox.
OH	4.86	1.80	ox.
e_{aq}^-	3.41	0.68	red.
H	0.87	0.52	red.
H^+	3.41	0.68	–
OH^-	0.00	0.00	–

25°C). The water temperature and the dissolved oxygen concentration were controlled to 288 ± 1°C and 10 ± 0.1 mg/dm^3, respectively. The dissolved amounts of YSZ were determined by the weight losses of YSZ.

3. Evaluation of water radiolysis

A computer simulation code for water radiolysis, SIMFONY [10,11], was applied for estimation of radiolysis species concentrations in the experimental apparatus. The G-values (primary yields) of radiolysis species listed in Table 2 were used as inputs for computer calculations. These values were derived from recent reports [5,7].

Calculation results are shown in Table 3 in comparison with values for 1100 MWe BWR core water. The radiation field of the experimental irradiation vessel was 2–3 orders of magnitude lower than that of a BWR core. Then, the dissolved oxygen concentration of the experimental vessel was set two orders of magnitude higher than in a BWR in order to get the concentrations of radiolysis species closer to those under BWR core conditions.

Table 3
Radiolysis calculation results

Species	Experimental apparatus		1100 MWe BWR
	irradiation	non-irr.	core
O_2	0.99×10^4 μg/l	1.0×10^4	150–350
H_2	5.7	< 0.1	5–80
H_2O_2	510	< 3	140–1000
O_2^-	2.3	< 0.05	3–13
HO_2^-	0.65	~ 0	0.2–1
OH	0.004	~ 0	0.1–0.5
HO_2	0.35	~ 0	0.5–2
e_{aq}^-	~ 0	~ 0	~ 0
H	~ 0	~ 0	~ 0

4. Experimental results and discussion

4.1. Corrosion weight gains and oxide film observations

Corrosion weight gains of test coupons were compared under conditions with and without irradiation as shown in Figs. 2–4. No nodular oxide was observed on any coupons. The weight gains of specimen A which had the lowest nodular corrosion resistance were lower for the γ-ray irradiation condition than the non-irradiation condition (Fig. 2). In the case of specimen B which had a medium resistance, the prefilmed coupons showed the similar tendency as specimen A, but the weight gains of non-prefilmed coupons were almost the same, with and without γ-ray irradiation (Fig. 3). In the case of specimen C which had the highest corrosion resistance, the weight gains were almost the same with and without irradiation for coupons both with and without the prefilm (Fig. 4). These weight gain differences between with and without irradiation were smaller for higher corrosion resistance alloys. It is commonly believed that irradiation enhances the corrosion of zirconium alloys. The lower corrosion weight gains for γ-ray irradiation seemed to contradict this common understanding. Then, the oxide film thicknesses after the 2400 h corrosion test were measured by SEM. They are compared in Table 4 with film thicknesses estimated from the weight gains. The ratios of the estimated thickness and measured thickness (θ_{WG}/θ_{SEM}) were smaller for the γ-ray irradiation specimens. We thought that some oxide film dissolution into water occurred during its growth. The amount of the dissolved oxide had to be higher for the γ-ray irradiation specimens to cause the lower values for the ratio of θ_{WG}/θ_{SEM}. The weight gain was more sensitive to the oxide film dissolution, since micro cracks and pores formed by the oxide dissolution had hardly any effect on the SEM-observed thickness.

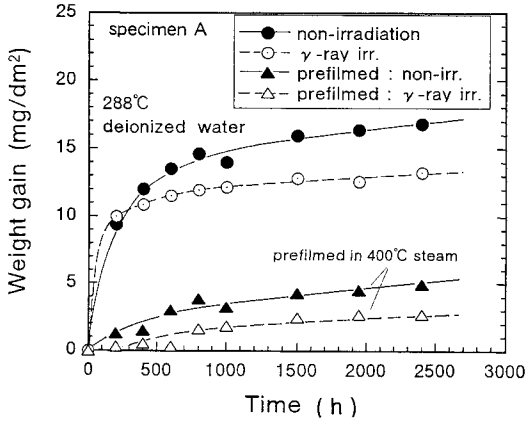

Fig. 2. Weight gains of specimen A in 288°C pure water with and without γ-ray irradiation.

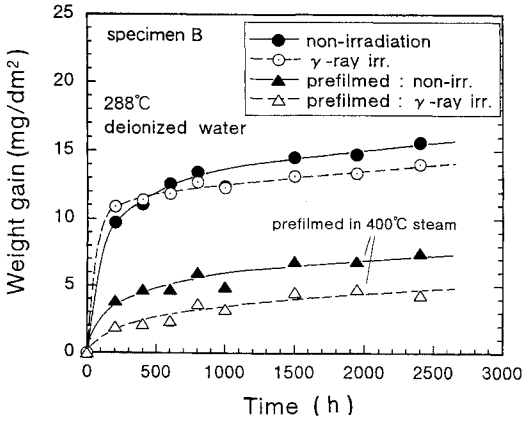

Fig. 3. Weight gains of specimen B in 288°C pure water with and without γ-ray irradiation.

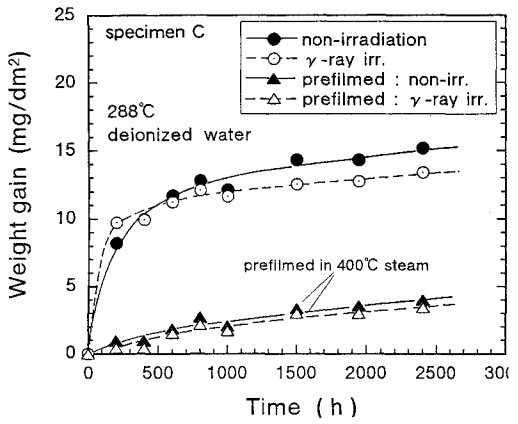

Fig. 4. Weight gains of specimen C in 288°C pure water with and without γ-ray irradiation.

In order to examine how the dissolution affected the oxide surface, the surface roughnesses of oxide films were measured by AFM and the values are also listed in Table 4. The average surface roughness R_a was larger on the irradiated surface than the non-irradiated surface. The γ-ray irradiation was considered to accelerate the oxide dissolution into high temperature water, making the surface rougher. The lowest corrosion resistance alloy (specimen A) had more dissolution of oxide film, especially in the case of γ-ray irradiation, which caused the largest weight gain difference between test coupons with and without irradiation and larger surface roughness on the irradiated surface. Surface observations on specimen A by SEM and AFM are shown in Fig. 5. The SEM photographs did not show much difference with and without γ-ray irradiation. On the other hand, the AFM images showed clearly that the irradiated coupon had a larger surface roughness. We thought that the water radiolysis species which were produced under γ-ray irradiation affected dissolution of the Zircaloy oxide film into water. Since the oxide film was not homogeneous, its dissolution was considered to proceed locally, such as at the oxide crystal grain boundary, to cause the larger surface roughness. Then, when this oxide film dissolution had proceeded, we thought the protective oxide film had been broken down which caused acceleration of the corrosion rate such as in the form of nodular oxides or a transition of uniform corrosion rate.

4.2. Changes in crystal structure of oxide films

Protective dense oxide films are known to contain tetragonal-ZrO_2 (t-ZrO_2), while monoclinic-ZrO_2 (m-

Table 4
Oxide film thickness and surface roughness after 2400 h corrosion test

	Specimens					
	A		B		C	
	γ-ray irradiation	non-irradiation	γ-ray	non.	γ-ray	non.
Film thickness from SEM, θ_{SEM} (μm)	1.03	1.14	1.06	0.99	1.08	0.97
Weight gain, W (mg/dm²)	13.3	16.8	14.0	15.6	13.4	15.2
Film thickness from weight gain [a], θ_{WG} (μm)	0.887	1.12	0.934	1.04	0.894	1.01
Film thickness difference, θ_{WG}/θ_{SEM} (%)	86	98	88	105	90	103
Average surface roughness [b], R_a (nm)	86.4	48.2	61.0	55.7	59.0	49.4
	A: prefilmed		B: prefilmed		C: prefilmed	
Growth film thickness from SEM, θ_{SEM} (μm)	0.44	0.60	0.41	0.56	0.28	0.33
Weight gain, W (mg/dm²)	2.69	4.93	4.34	7.51	3.44	3.99
Film thickness from weight gain [a], θ_{WG}(μm)	0.179	0.329	0.289	0.501	0.229	0.266
Film thickness difference, θ_{WG}/θ_{SEM} (%)	41	55	70	89	82	81
Average surface roughness [b], R_a (nm)	96.3	85.1	87.7	80.9	80.1	77.5

[a] $\theta_{WG} = W/15$, 1 μm film thickness ≒ 15 mg/dm² weight gain.
[b] Measured by atomic force microscope (AFM) on 20 μm square × 5 points.

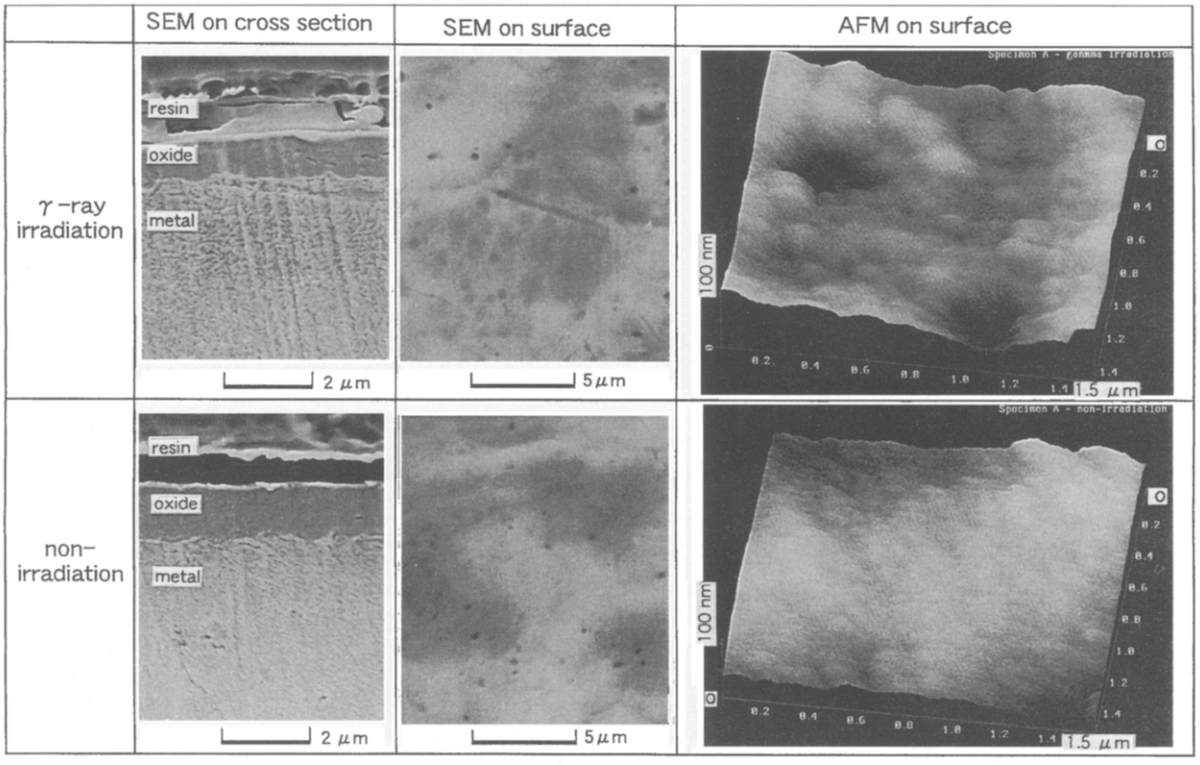

Fig. 5. SEM and AFM observations on non-prefilmed specimen A after 2400 h corrosion test.

ZrO_2) is stable thermodynamically [1,12–14]. Low angle incident XRD was used to determine the crystal structure of the oxide film. Lower incident angles provide information on the outer surface structure of the oxide film as shown in Fig. 6. The diffraction of one degree incident X-rays is 99% from about the 1.2 μm depth oxide film due to X-ray absorption (see for example Ref. [15]). The signals at $2\theta = 30.1$ and $2\theta = 28.1°$ represented the t-ZrO_2 (101) and m-ZrO_2 ($\bar{1}11$) peaks, respectively. The intensity ratio of these two peaks (I_{t-ZrO_2}/I_{m-ZrO_2}) is plotted as a function of the X-ray incident angle in Fig. 6(b). Lower values of I_{t-ZrO_2}/I_{m-ZrO_2} were obtained for the γ-ray irradiated coupons. The outer surface of the oxide film contained less t-ZrO_2, especially in the case of γ-ray

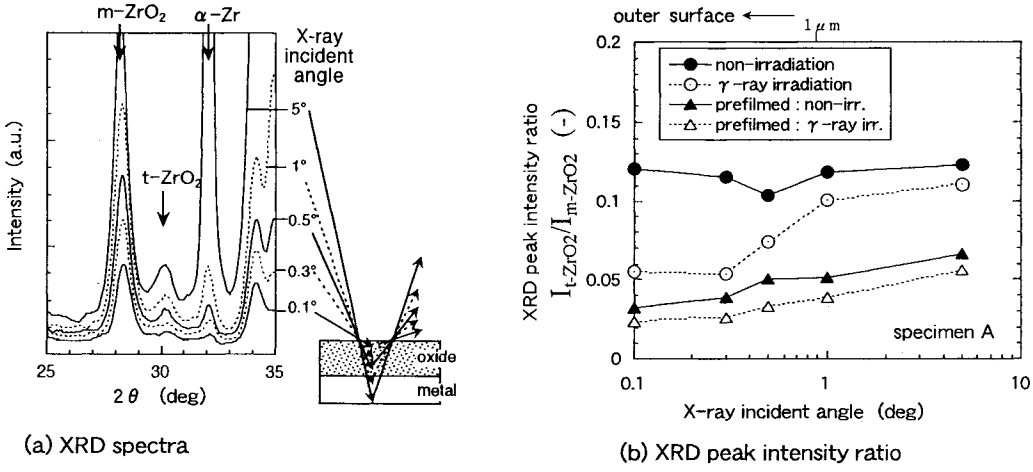

Fig. 6. X-ray diffraction (XRD) analysis of oxide films on specimen A after 200 h.corrosion test. (a) XRD spectra of γ-ray-irradiated sample. (b) Peak intensity ratio of tetragonal- and monoclinic-ZrO_2 as a function of X-ray incident angle.

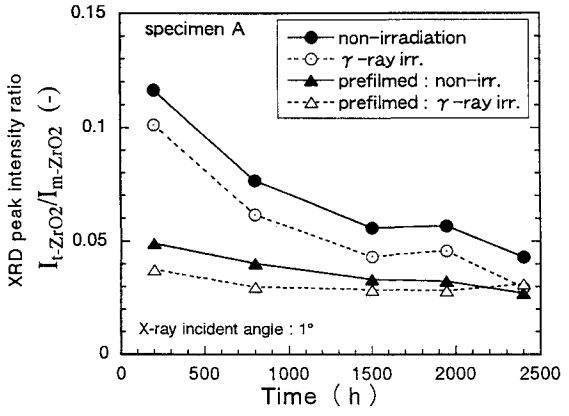

Fig. 7. XRD peak ratio of tetragonal- and monoclinic-ZrO_2 as a function of corrosion time.

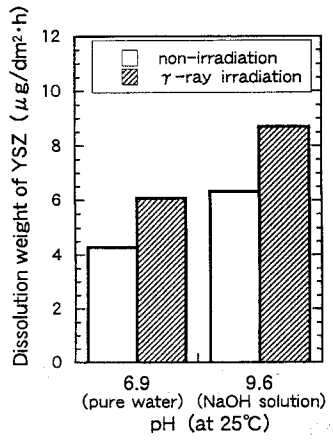

Fig. 8. Dissolution of single crystal yttria-doped ZrO_2 in 288°C pure water.

irradiated non-prefilmed coupon. The same tendency was observed for all other specimens. We thought that the oxide film dissolution into water proceeded at the outer surface of the oxide film and this dissolution caused the smaller t-ZrO_2 content. We could not determine whether the preferential dissolution of t-ZrO_2 occurred or if the dissolution induced the transformation of t-ZrO_2 to m-ZrO_2 from these experiments.

Fig. 7 shows the ratios of I_{t-ZrO_2}/I_{m-ZrO_2} measured on specimen A as a function of corrosion time. The t-ZrO_2 content decreased as the corrosion time proceeded. This was also due to the film dissolution. However, the t-ZrO_2 remained at the metal–oxide interface where the barrier oxide film was believed to exist. Then, the ratios of I_{t-ZrO_2}/I_{m-ZrO_2} seemed to saturate at almost the same values.

4.3. Dissolution of zirconium oxide

In order to confirm the enhancement of the oxide film dissolution under γ-ray irradiation, dissolution experiments of single crystal zirconium oxide (YSZ) were performed in 288°C water. Fig. 8 shows the dissolution amounts of YSZ at pH 6.9 (deionized water) and pH 9.6 (NaOH solution) both with and without γ-ray irradiation. The dissolution amounts of YSZ were about 30–40% larger for the γ-ray irradiation. This supported our hypothesis that γ-rays enhanced dissolution of zirconium oxide film. The dissolution amounts were larger at pH 9.6. This was because solubility of ZrO_2 became larger at higher pH. Cox and Wu [9,9] reported the dissolution of the oxide film on Zircaloy in LiOH alkaline solutions.

Pourbaix [16] proposed a ZrO_2–H_2O equilibrium system. The lowest solubility of ZrO_2 is obtained at about pH 6.6 in 25°C water. The solubility is larger at both lower and higher pH:

$$ZrO_2 + 2H^+ = ZrO^{2+} + H_2O, \quad pH < 6.6,$$

$$ZrO_2 + OH^- = HZrO_3^-, \quad pH > 6.6.$$

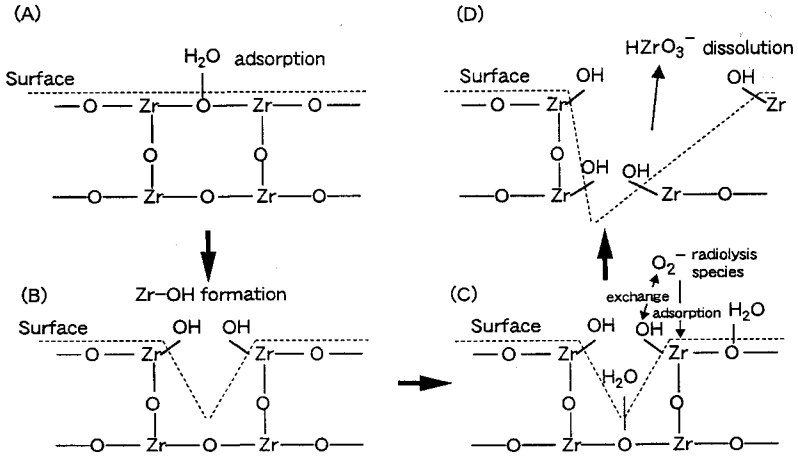

Fig. 9. Model of dissolution process of zirconium oxide film into water.

The degradation process of YSZ has been studied in high temperature water [17–19]. Yoshimura et al. [17] and Sato and Shimada [18] proposed similar transformation models of yttria-doped tetragonal-ZrO_2 to monoclinic in which the t- to m-ZrO_2 transformation was induced by the stress migration due to micro-cracks which were produced by the dissolution of ZrO_2 into water. A similar transformation could occur at oxide films on Zircaloy as shown in Fig. 9. The dissolution of ZrO_2 would generate the micro-cracks at the oxide film to cause the t- to m-ZrO_2 transformation observed in Figs. 6 and 7. The water radiolysis species accelerated the dissolution of the Zircaloy oxide film, especially the film on an alloy with lower nodular corrosion resistance. When the oxide film dissolution proceeds, it would cause a breakdown of the barrier oxide film and this breakdown would be one of the factors controlling nucleation of the nodular oxides.

5. Conclusion

Laboratory corrosion tests for three different zirconium alloys were performed in 288°C oxygenated pure water for 100 days both with and without ^{60}Co γ-ray irradiation. The zirconium alloys were based on Zircaloy-2. No nodular oxide was observed on any coupons. Corrosion weight gains of the alloy which had a lower nodular corrosion resistance were lower for the irradiation condition than the non-irradiation condition. On the other hand, the alloys which had a higher nodular corrosion resistance showed almost the same weight gains for both conditions. Differences of weight gain with and without irradiation were attributed to dissolution of oxide film in the high temperature water. Low angle incident X-ray diffraction analysis showed that the tetragonal-ZrO_2 fraction in oxide film was lower with irradiation than without it. The water radiolysis species were considered to accelerate the dissolution of oxide film, especially film on alloys with lower nodular corrosion resistance. This dissolution was considered to cause the lower tetragonal-ZrO_2 fraction at the oxide film surface. This water radiolysis enhanced dissolution was confirmed by the dissolution tests of single crystal yttria-doped ZrO_2 which showed 30–40% larger dissolution under the γ-ray irradiation. This oxide film dissolution was considered to be one of the factors leading to a localized breakdown of the barrier oxide film, before forming the nodular oxide.

References

[1] Corrosion on Zirconium Alloys in Nuclear Power Plants, International Atomic Energy Agency, TECDOC-684, 1993.
[2] W.G. Burns, P.B. Moore, Radiat. Eff. 30 (1976) 233.
[3] W.G. Burns, P.B. Moore, Proc. Chemistry of Nuclear Reactor Systems, Bournemouth, England, Oct. 1977 (BNES, London, 1978) p. 281.
[4] Y. Katsumura, S. Yamamoto, D. Hiroishi, K. Ishigure, M. Washio, Radiat. Phys. Chem. 39 (1992) 383.
[5] G.R. Sunaryo, Y. Katsumura, D. Hiroishi, K. Ishigure, Radiat. Phys. Chem. 45 (1995) 131.
[6] G.V. Buxton, C.L. Greenstock, W.P. Helman, A.B. Ross, J. Phys. Chem. Raf. Data 17 (1988) 513.
[7] A.J. Elliot, D.R. MacCracken, G.V. Buxton, N.D. Wood, J. Chem. Soc. Faraday Trans. 86 (1990) 1539.
[8] B. Cox, C. Wu, J. Nucl. Mater. 199 (1993) 272.
[9] B. Cox, C. Wu, J. Nucl. Mater. 224 (1995) 169.
[10] E. Ibe, S. Uchida, J. Nucl. Mater. 130 (1985) 45.
[11] E. Ibe, M. Sakagami, S. Uchida, J. Nucl. Sci. Technol. 24 (1987) 220.
[12] J. Godlewski, J.P. Gros, M. Lambertin, J.F. Wadier, H. Weidinger, ASTM-STP 1132 (ASTM, Philadelphia, PA, 1991) p. 416.
[13] H.J. Beie, A. Mitwalsky, F. Garzarolli, H. Ruhmann, H.J. Sell, ASTM-STP 1245 (ASTM, Philadelphia, PA, 1994) p. 615.
[14] J. Godlewski, ASTM-STP 1245 (ASTM, Philadelphia, PA, 1994) p. 663.
[15] B.D. Cullity, Elements of X-ray Diffraction, 2nd Ed. (Addison-Wesley, Massachusetts, 1978) ch. 9.
[16] M. Pourbaix, Atlas of Electrochemical Equilibria (Pergamon, London, 1966) p. 223.
[17] M. Yoshimura, T. Noma, K. Kawabata, S. Somiya, J. Mater. Sci. Lett. 6 (1987) 456.
[18] T. Sato, M. Shimada, J. Am. Ceram. Soc. 68 (1985) 356.
[19] M. Yoshimura, T. Hiuga, S. Somiya, J. Am. Ceram. Soc. 69 (1986) 583.